JACS
JOURNAL OF THE AMERICAN CHEMICAL SOCIETY
Article
pubs.acs.org/JACS

Hierarchically Structured Free-Standing Hydrogels with Liquid Crystalline Domains and Magnetic Nanoparticles as Dual Physical Cross-Linkers

Yuxiang Zhou,[†] Nitin Sharma,[‡] Prashant Deshmukh,[†] Rubinder Kaur Lakhman,[‡] Menka Jain,[§,∥] and Rajeswari M. Kasi*[,†,‡]

[†]Department of Chemistry, [‡]Polymer Program, Institute of Materials Science, [§]Department of Physics, and [∥]Institute of Materials Science, University of Connecticut, Storrs, Connecticut 06269, United States

Supporting Information

ABSTRACT: Here we report a modular strategy for preparing physically cross-linked and mechanically robust free-standing hydrogels comprising unique thermotropic liquid crystalline (LC) domains and magnetic nanoparticles both of which serve as the physical cross-linkers resulting in hydrogels that can be used as magnetically responsive soft actuators. A series of amphiphilic LC pentablock copolymers of poly(acrylic acid) (PAA), poly(5-cholesteryloxypentyl methacrylate) (PC5MA), and poly(ethylene oxide) (PEO) blocks in the sequence of PAA−PC5MA−PEO−PC5MA−PAA were prepared using reversible addition−fragmentation chain transfer polymerization. These pentablock copolymers served as macromolecular ligands to template Fe_3O_4 magnetic nanoparticles (MNPs), which were directly anchored to the polymer chains through the coordination bonds with the carboxyl groups of PAA blocks. The resulting polymer/MNP nanocomposites comprised a complicated hierarchical structure in which polymer-coated MNP clusters were dispersed in a microsegregated pentablock copolymer matrix that further contained LC ordering. Upon swelling, the hierarchical structure was disrupted and converted to a network structure, in which MNP clusters were anchored to the polymer chains and LC domains stayed intact to connect solvated PEO and PAA blocks, leading to a free-standing LC magnetic hydrogel (LC ferrogel). By varying the PAA weight fraction (f_{AA}) in the pentablock copolymers, the swelling degrees (Q) of the resulting LC ferrogels were tailored. Rheological experiments showed that these physically cross-linked free-standing LC ferrogels exhibit good mechanical strength with storage moduli G' of around 10^4−10^5 Pa, similar to that of natural tissues. Furthermore, application of a magnetic field induced bending actuation of the LC ferrogels. Therefore, these physically cross-linked and mechanically robust LC ferrogels can be used as soft actuators and artificial muscles. Moreover, this design strategy is a versatile platform for incorporation of different types of nanoparticles (metallic, inorganic, biological, etc.) into multifunctional amphiphilic block copolymers, resulting in unique free-standing hybrid hydrogels of good mechanical strength and integrity with tailored properties and end applications.

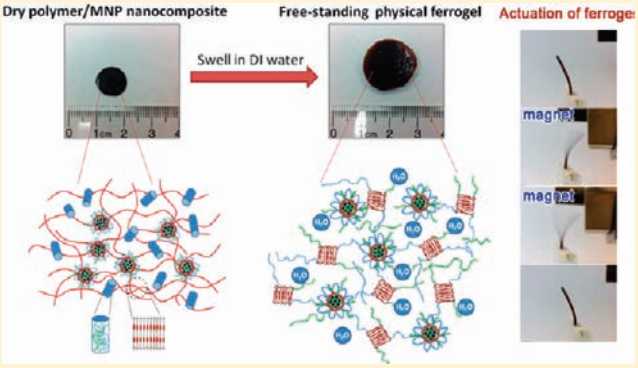

INTRODUCTION

Polymeric hydrogels are an appealing category of soft materials due to their tunable water content as well as their application-dependent mechanical properties.[1,2] By tailoring the functionalities of the polymer networks, responsive hydrogels that are sensitive to temperature, light, pH, ionic strength, or bioactive species can be obtained.[2−10] The three-dimensional network structures of hydrogels can also be used as the scaffolds to incorporate various nanoparticles (metallic, inorganic, bioactive, etc.), resulting in hybrid hydrogels with enhanced mechanical properties or/and unique optical, electric, magnetic, or biological properties.[11−17] Specifically, introducing magnetic nanoparticles (MNPs) into hydrogels leads to magnetic hydrogels or ferrogels, which are sensitive to an external magnetic field. This allows noncontact triggering of hydrogels, including shape deformation or swelling/deswelling process. Because of this unique property, ferrogels have so far found applications in drug delivery, soft actuators, and artificial muscles.[18−22]

Ferrogels can be prepared by cross-linking hydrophilic monomers in the presence of an aqueous solution of MNPs stabilized with ligands (ferrofluid).[23−26] This approach usually leads to unstable mixtures where nanoparticles tend to diffuse out from the hydrogel network during the swelling−deswelling processes due to the lack of strong interactions between the nanoparticles and the polymer chains. To address this problem, MNPs can be directly attached to the polymer network through

Received: September 4, 2011
Published: December 26, 2011

   dx.doi.org/10.1021/ja208349x | J. Am. Chem.Soc. 2012, 134, 1630−1641

Scheme 1. Synthesis of Pentablock Copolymers PB20−C5MA$_x$−AA$_y$[a]

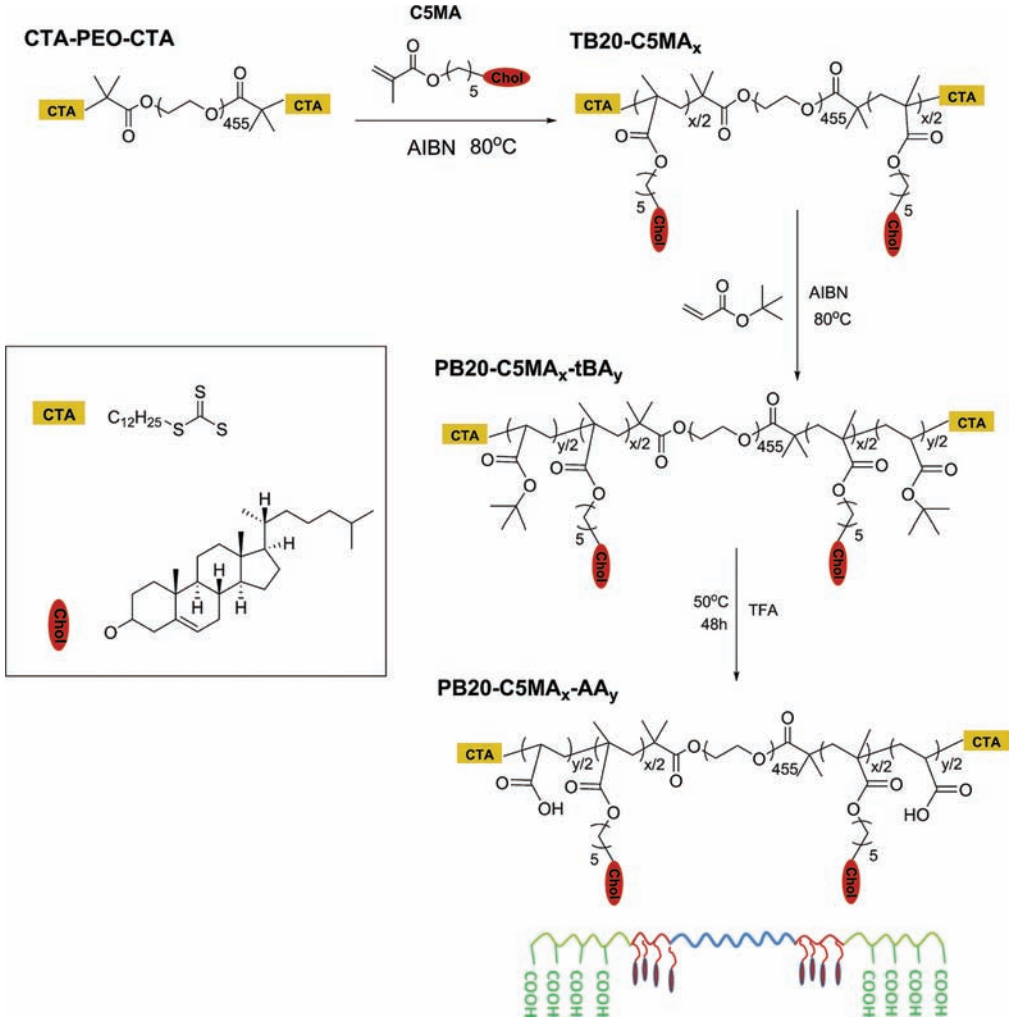

[a] M_n of PEO block is 20 kg/mol (DP = 455); x and y represent the degree of polymerization of the LC block and PAA block, respectively.

covalent bonds. This has been done by functionalizing the surface of MNPs with polymerizable vinyl groups and then copolymerizing them with hydrophilic monomers at the aid of a multifunctional monomer (cross-linker) or by preparing multifunctionalized MNPs and using them as the cross-linker to cure the hydrophilic monomers.[27−31] These strategies lead to chemically cross-linked ferrogel networks that afford good mechanical properties and good structural integrity so that the MNPs will not be leached out during the use of the materials.[32] However, chemically cross-linked hydrogel networks cannot be processed or reprocessed. Moreover, the use of a single type of hydrophilic monomer results in a purely hydrophilic system that cannot be used in applications like encapsulating and delivering hydrophobic drug molecules.

In contrast to chemically cross-linked hydrogels, physically cross-linked hydrogels are connected by noncovalent junctions formed through hydrophobic interactions, ionic interactions, hydrogen bonding, or host−guest complexes.[33−40] These "temporary" junctions can lead to reversible sol−gel or gel−sol transitions, which not only allow the prepared hydrogels to be processable, but also facilitate the stimuli-responsive behaviors of the hydrogels. Nevertheless, although some physically cross-linked organogels comprising MNPs have been prepared,[41−43] there are very few examples in the literature regarding MNPs incorporated into a physical hydrogel network. Qin et al. have prepared a physical ferrogel by incorporating oleic acid-coated Fe_3O_4 MNPs into a Pluronics (PEO−PPO−PEO) aqueous solution.[44] Above a critical temperature and concentration, the solution will undergo a sol−gel transition due to the micellization of the PEO−PPO−PEO chains, resulting in a physical ferrogel with MNPs encapsulated in the PPO hydrophobic domains. This thermoreversible physical ferrogel can be used as an injectable drug delivery system in which the drug release can be triggered by applying a magnetic field. However, in this physical ferrogel, MNPs are only encapsulated within the hydrogel network through hydrophobic interactions with PPO, and the mechanical strength of this physical ferrogel is also relatively low. It should be noted that for applications such as soft actuators or artificial muscles, free-standing hydrogels with much better mechanical properties are desired.[45] Recently, Bailey et al. have prepared free-standing physical hydrogels by swelling melt blends of PS−PEO−PS triblock copolymer and PS−PEO diblock copolymer in DI water.[46] The spherical glassy PS domains preformed in the melt state remain vitrified and dehydrated during swelling and are tethered by the PS−PEO−PS polymer chains, so that they can serve as physical cross-linkers to hold the integrity of the resulting hydrogel. This

dx.doi.org/10.1021/ja208349x | J. Am. Chem.Soc. 2012, 134, 1630−1641

Table 1. Composition of the Pentablock Copolymers

precursor pentablock copolymer	$M_{n,\ precursor}$[a]	$PDI_{precursor}$[a]	final pentablock copolymer	DP of AA[b]	DP of C5MA[b]	wt % of AA[b]
PB20−C5MA$_{35}$−tBA$_{76}$	36 390	1.26	PB20−C5MA$_{35}$−AA$_{76}$	76	35	12
PB20−C5MA$_{30}$−tBA$_{116}$	33 494	1.29	PB20−C5MA$_{30}$−AA$_{116}$	116	30	19
PB20−C5MA$_{30}$−tBA$_{223}$	41 274	1.36	PB20−C5MA$_{30}$−AA$_{223}$	223	30	31

[a] M_n and PDI were determined with precursor pentablock copolymers. [b] DP of AA and C5MA, as well as weight fractions of AA in PB20−C5MA$_x$−AA$_y$ were calculated from the integrals in the ^{1}H NMR spectra of the precursor pentablock copolymers since the TFA-catalyzed hydrolysis of PtBA was selective and quantitative.

approach provides physical hydrogels with mechanical properties comparable to chemically cross-linked hydrogels, yet this mechanically robust physical hydrogel is reprocessable.

Herein we report a modular strategy for preparing robust free-standing physical ferrogels by swelling the melt samples of a series of polymer/MNP nanocomposites in water. The nanocomposites were prepared through a convenient one-pot process, in which liquid crystalline (LC) pentablock copolymers containing poly(acrylic acid) (PAA) blocks served as macromolecular ligands to stabilize the freshly made Fe_3O_4 MNPs in situ. The melt sample of polymer/MNP nanocomposite encompassed a complicated hierarchical structure where polymer-coated MNP clusters were embedded in the block copolymer microsegregated matrix consisting of hydrophilic domains and LC domains. Upon swelling in water, the hierarchical structure was disrupted and converted to a hydrogel network connected by LC domains as physical cross-linkers; the embedded MNP clusters not only provide the magnetic susceptibility but also served as the metallic fillers and possibly the second physical cross-linker in addition to the LC domains. The resulting ferrogels are different from conventional physical hydrogels in that they are free-standing and display good mechanical strength similar to chemically cross-linked hydrogels, yet they can still be reprocessed. Furthermore, the swelling degrees along with the mechanical properties of the ferrogels can be easily tuned by varying the PAA content in the polymer. These mechanically robust free-standing ferrogels can be used as soft actuators or artificial muscles. Moreover, this study offers a promising and versatile approach of templating various nanoparticles using the multifunctional amphiphilic block copolymers as a scaffold, affording hierarchically structured free-standing hybrid hydrogel networks with unique properties.

RESULT AND DISCUSSION

Synthesis and Characterization of Pentablock Copolymers. Amphiphilic LC pentablock copolymers comprised of poly(5-cholesteryloxymethacrylate) (PC5MA), poly(ethylene oxide) (PEO), and poly(acrylic acid) (PAA) blocks, in the sequence of PAA−PC5MA−PEO−PC5MA−PAA were carefully designed such that (1) PC5MA with side-chain cholesteryl mesogens affords hydrophobicity and LC properties, (2) PEO provides hydrophilicity, and (3) PAA provides hydrophilicity and has carboxyl groups which can bind to MNPs through coordination bonds (Scheme 1). These pentablock copolymers with 20 kg/mol PEO central block are labeled as PB20−C5MA$_x$−AA$_y$, where x and y stand for the degree of polymerization (DP) of the LC block and PAA block, respectively (Scheme 1).

The synthetic strategy to prepare PB20−C5MA$_x$−AA$_y$ by reversible addition-fragmentation chain transfer (RAFT) polymerization is illustrated in Scheme 1 and the experimental details are included in the Supporting Information. First, a telechelic PEO with trithiocarbonate end groups (CTA−PEO−CTA) was synthesized from a published procedure.[47] Second, the LC monomer 5-cholesteryloxypentyl methacrylate (C5MA), where the cholesteryl mesogen was attached to the polymerizable methacrylate moiety via a soft methylene spacer, was prepared as reported.[48] Third, CTA−PEO−CTA was used as the macromolecular chain transfer agent (macro-CTA) in the polymerization of C5MA, resulting in the triblock copolymer (TB20−C5MA$_x$, where x is the DP of C5MA). Two batches of TB20−C5MA$_x$ have been prepared, and the DP values of C5MA were found to be 35 and 30, respectively, by using ^{1}H NMR. Fourth, the triblock copolymers TB20−C5MA$_x$ retained the trithiocarbonate end groups and thus were used as the macro-CTA for the polymerization of *tert*-butyl acrylate (tBA), resulting in precursor pentablock copolymers (PB20−C5MA$_x$−tBA$_y$), where x and y stand for the DP of C5MA and AA, respectively. In the last synthetic step, the precursor pentablock copolymers were treated with trifluoroacetic acid (TFA) to remove the *tert*-butyl groups, resulting in the final pentablock copolymers PB20−C5MA$_x$−AA$_y$. It should be noted that the selective and quantitative hydrolysis of PtBA catalyzed by TFA in various copolymers has been previously reported.[49−52] The ^{1}H NMR spectra of PB20−C5MA$_x$−AA$_y$ also showed the complete disappearance of the resonance of the *tert*-butyl group while the resonance for the ester linkage that connect polymer backbone and the methylene spacer is preserved (Figure S1, Supporting Information), suggesting that the hydrolysis of PtBA is quantitative and the side-chain cholesteryl groups were retained and intact after hydrolysis. Therefore, the DP of AA in the final pentablock copolymers equals the DP of tBA in the precursor pentablock copolymers, and the DP of the C5MA remained the same after TFA-catalyzed hydrolysis.

The compositions of the precursor and final pentablock copolymers were determined by ^{1}H NMR (Figure S1, Supporting Information). The number average molecular weight (M_n) and the polydispersity indices (PDI) of precursor pentablock copolymers, PB20−C5MA$_x$−tBA$_y$, were measured by gel permeation chromatography (GPC) (Figure S2, Supporting Information). GPC analysis of final pentablock copolymer, PB20−C5MA$_x$−AA$_y$ was not investigated because the charged carboxyl groups of PAA adsorbed to the immobile phase of the GPC column. The chemical compositions of pentablock copolymers are summarized in Table 1.

Preparation and Characterization of the Polymer/MNP Nanocomposites. The polymer/MNP nanocomposites that were to be used to prepare swollen ferrogels were attained by incorporating the MNPs into the LC pentablock copolymers PB20−C5MA$_x$−AA$_y$ through the coordination bonds between carboxyl groups and the surface of MNPs. The composition of these nanocomposites was carefully designed such that (1) during swelling the hydrophobic LC domains formed by ordered cholesteryl mesogens function as junctions that

dx.doi.org/10.1021/ja208349x | J. Am. Chem.Soc. 2012, 134, 1630−1641

connect solvated PAA and PEO blocks in water, forming a swollen hydrogel network, and (2) the templated MNPs not only provide the magnetic field susceptibility but as also function as the secondary cross-linkers to enhance the mechanical properties of the resulting ferrogels. The preparation of the polymer/MNP nanocomposites can be summarized as two steps: (1) in situ stabilization of Fe_3O_4 MNPs in aqueous solution using pentablock copolymers PB20−C5MA$_x$−AA$_y$ as macromolecular ligands and (2) freeze-drying of the resulting solution to give melt sample of polymer/MNP nanocomposite, which was subsequently processed by compression molding to give a discoid sample for making the swollen ferrogel. The detailed preparation and characterization are discussed in following sections.

In Situ Stabilization of MNPs with Pentablock Copolymers in Aqueous Solution. MNPs were first prepared through the coprecipitation of ferrous and ferric ions ($[Fe^{2+}]$:$[Fe^{3+}]$ = 1:2) in an alkaline solution. The dioxane solution of PB20−C5MA$_x$−AA$_y$ was then added into the resulting MNP aqueous suspension and behaved as a macromolecular ligand to stabilize the MNPs. Dioxane and other small molecules were subsequently removed through dialysis, and a black-colored aqueous solution containing polymer stabilized MNPs was obtained (hereafter known as polymer/MNP solution). The prepared polymer/MNP solution stayed homogeneous without visible precipitation when kept on the benchtop for more than 1 month, suggesting that the pentablock copolymers effectively stabilized the MNPs. The approach used here is a facile one-pot process to make the polymer/MNP nanocomposite. The pentablock copolymers were added in situ when the MNPs were synthesized. Comparing to the reported procedures in which MNPs are first stabilized by small molecular surfactant (i.e., oleic acid) and then mixed or reacted with polymers, the approach applied here is more convenient.

For each pentablock copolymer PB20−C5MA$_x$−AA$_y$, a corresponding polymer/MNP solution has been prepared, labeled as PB20−C5MA$_x$−AA$_y$/MNP. Here it is not intended to study how the variation of the MNP content will affect the properties of resulting ferrogels, and thus the feed ratio of the ferrous and ferric ions with respect to PB20−C5MA$_x$−AA$_y$ is fixed for all three nanocomposites. It should be noted here that, although three nanocomposites have been prepared, PB20−C5MA$_{30}$−AA$_{116}$/MNP nanocomposite was used for comprehensive structural, thermal, and morphological characterizations reported in this publication, while PB20−C5MA$_{35}$−AA$_{76}$/MNP and PB20−C5MA$_{30}$−AA$_{223}$/MNP were mainly studied for their swelling behaviors and gel properties and compared with the PB20−C5MA$_{30}$−AA$_{116}$/MNP nanocomposite.

Because the membrane used for dialysis has a molecular weight cutoff of about 3000 Da, which is well below the M_n of the pentablock copolymers, the prepared polymer/MNP solution should comprise both the micelles encapsulating MNPs (hereafter referred as MNP micelles) and unbonded pentablock copolymers. Dynamic light scattering (DLS) experiments were performed on PB20−C5MA$_{30}$−AA$_{116}$/MNP solution to confirm the presence of both populations. A magnet was placed at the bottom of the vial containing the PB20−C5MA$_{30}$−AA$_{116}$/MNP solution, and the MNP micelles were attracted to the bottom. The supernatant was then decanted and separated from the MNP micelles. The collected MNP micelles were redissolved in DI water, and both the resulting MNP micelle solution and the supernatant were analyzed by DLS. Figure 1 shows the DLS results of the MNP micelles and the supernatant. It is observed that the hydrodynamic radius (R_H) of the MNP micelles is around 99 nm. The size distribution of the MNP micelles is unimodal and relatively narrow, indicating that the pentablock copolymers formed well-defined micellar structure encapsulating MNPs. In the DLS result of the supernatant, nanoparticles of R_H equal to ∼48 nm are also observed, suggesting that the unbonded amphiphilic pentablock copolymers PB20−C5MA$_{30}$−AA$_{116}$ also self-assemble to form micellar structures in the aqueous solution (plain polymer micelles). The size of the plain polymer micelles is smaller than that of MNP micelles, since they do not contain MNPs. Therefore, the DLS study demonstrates the coexistence of both the MNP micelles and plain polymer micelles in the polymer/MNP solution.

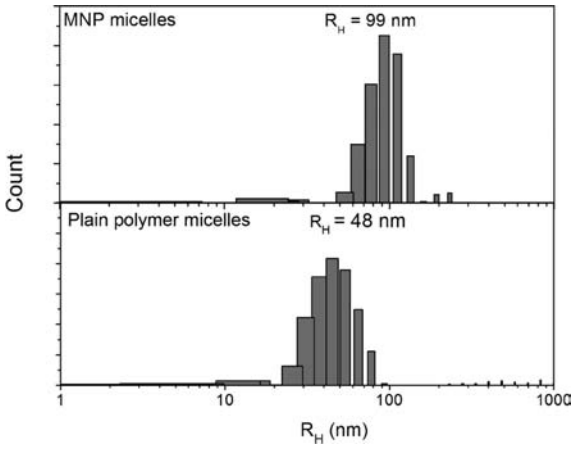

Figure 1. DLS results of the MNP micelles and the supernatant containing plain polymer micelles.

Transmission electron microscopy (TEM) was also used to analyze the polymer/MNP samples. In the first set of experiments, samples were prepared by casting the polymer/MNP solution on Formvar-coated copper grids. The samples were directly used without further staining; thus, the pentablock copolymers (including the polymer coating of the MNP micelles and the plain polymer micelles) are not discernible due to their low electron density. Figure 2a is the broad range image of PB20−C5MA$_{30}$−AA$_{116}$/MNP, in which only clusters of MNPs can be observed. Most MNP clusters are around 50−100 nm in diameter, while some MNP clusters are as large as ∼200 nm. It is inferred that the former reflects the actual sizes of MNP clusters in the solution which are stabilized by the pentablock copolymers, and the latter is likely formed during the drying process when the small MNP clusters agglomerate together due to their inherent magnetic attraction force. It is noted that the size of the MNP clusters observed in TEM (diameter = 50−100 nm) is smaller than the size of the MNP micelles identified by DLS (R_H = 99 nm, diameter = 198 nm), and this is attributed to the polymer coating surrounding the MNP clusters not being discernible in the TEM. In the zoomed-in TEM image (Figure 2b), boundaries between individual MNPs were noted, suggesting that PAA chains surround MNPs and prevent them from collapsing together. The size of the individual MNP was identified with image analysis software (ImageJ) and was found to be ∼12 nm in diameter on average. By combining the results of TEM and DLS, the structure of the MNP micelles can be constructed as illustrated in Figure 2c. The PAA chains bind to/bridge multiple MNPs through the coordination bonding between the

dx.doi.org/10.1021/ja208349x | J. Am. Chem.Soc. 2012, 134, 1630−1641

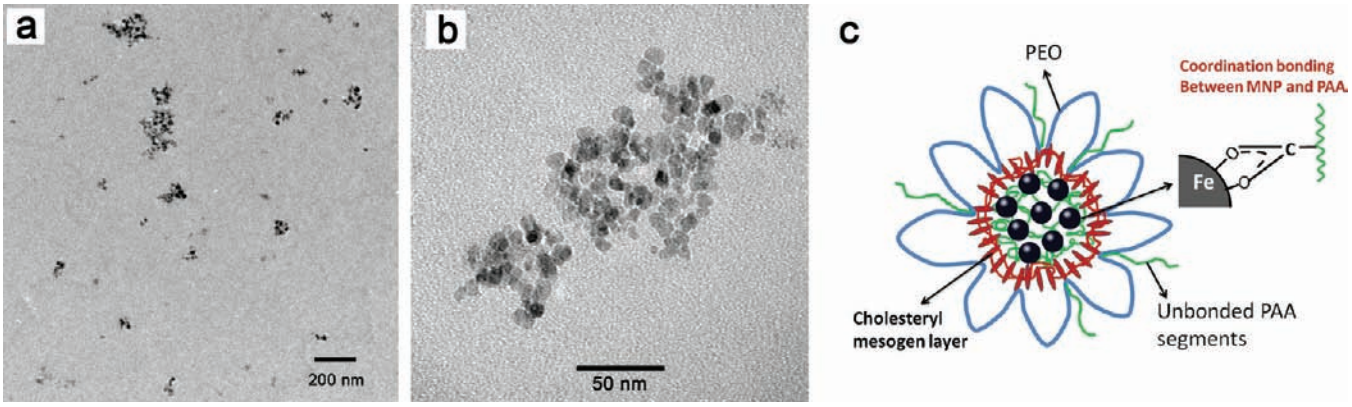

Figure 2. (a) Broad range TEM image and (b) zoomed-in TEM image of PB20−C5MA$_{30}$−AA$_{116}$/MNP. The TEM sample was prepared by solution-casting the PB20−C5MA$_{30}$−AA$_{116}$/MNP solution on a copper grid coated by Formvar film. (c) Schematic illustration of MNP micelles with a multilayered structure.

MNP surface and carboxyl groups.[53−56] The LC blocks self-assembled to form a hydrophobic cholesteryl mesogen layer surrounding the PAA-coated MNP clusters due to the strong hydrophobic interaction of the cholesteryl mesogens in the aqueous environment, while the PEO blocks formed the outer layer to provide the steric effects to prevent the further aggregation of the MNP clusters. We also expect some unbonded PAA segments to remain in the corona in the vicinity of PEO chains due to their hydrophilicity.

Preparation and Characterization of the Melt Sample of the Polymer/MNP Nanocomposite. As discussed previously, the prepared polymer/MNP solution comprised both the MNP micelles and plain polymer micelles. Without removing the plain polymer micelles, the polymer/MNP solution was directly freeze-dried. The freeze-dried sample was then subjected to the compression molding process at 100 °C for 1 h to give a discoid sheet sample, which was later used to prepare swollen ferrogels. In the resulting dry polymer/MNP nanocomposites, on one hand, the multilayered structure of the MNP micelles should be retained because polymers are strongly anchored to the surface of MNPs through coordination bonds, though the PAA and PEO layers should shrink or collapse due to the loss of water. On the other hand, the unbonded polymer chains undergo a phase transition from the micellar structure in solution to the melt state structure. The detailed structure analysis of the dry polymer/MNP nanocomposite will be discussed in the subsequent sections.

A vibrating sample magnetometer was used to confirm the superparamagnetic properties of the polymer/MNP nanocomposites. It is well-documented that Fe_3O_4 nanoparticles exhibit superparamagnetic properties below a critical size of 25 nm.[57] The size of the MNPs in the current study was found to be ∼12 nm by TEM, which falls below this size limit, and hence, superparamagnetic nature was expected. For example, Figure 3 shows the magnetization versus applied magnetic field plot for the PB20−C5MA$_{30}$−AA$_{116}$/MNP nanocomposite at 300 K. The measurement clearly shows that the sample has zero coercivity and remanence, which is consistent with the superparamagnetic behavior.[58] The saturation magnetization of MNPs embedded in PB20−C5MA$_{30}$−AA$_{116}$/MNP was found to be 46 emu/g Fe_3O_4. Saturation magnetization ranging between 30 and 60 emu/g Fe_3O_4 has been reported for MNPs with similar sizes in the literature.[53,59]

Using thermogravimetric analysis (TGA), the detailed composition information was obtained including (1) the weight fraction of the neat Fe_3O_4 MNPs (Φ_{MNP}) in the polymer/MNP nanocomposites and (2) the weight fraction of MNP micelles ($\Phi_{micelle}$) in the polymer/MNP nanocomposites. Figure 4 shows the TGA traces of plain polymer PB20−C5MA$_{30}$−AA$_{116}$ and PB20−C5MA$_{30}$−AA$_{116}$/MNP nanocomposite as an example. The polymer fraction was completely burned off

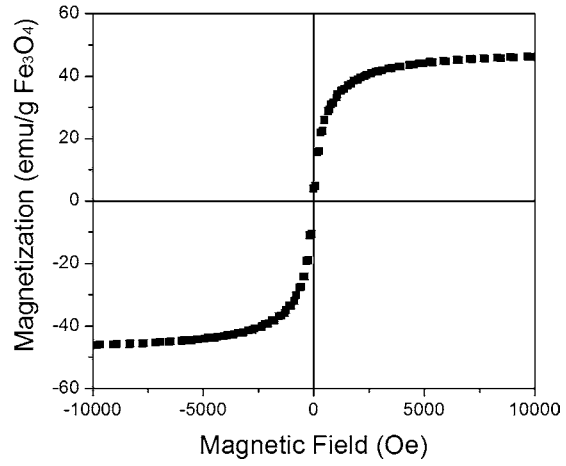

Figure 3. Magnetization versus applied magnetic field for the PB20−C5MA$_{30}$−AA$_{116}$/MNP nanocomposite.

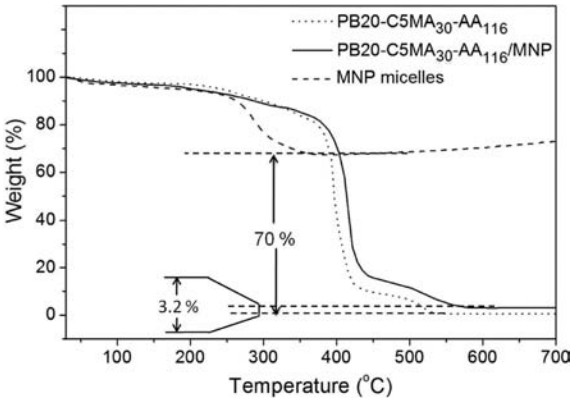

Figure 4. TGA traces of polymer PB20−C5MA$_{30}$−AA$_{116}$, PB20−C5MA$_{30}$−AA$_{116}$/MNP nanocomposite, and the corresponding MNP micelles.

dx.doi.org/10.1021/ja208349x | J. Am. Chem.Soc. 2012, 134, 1630−1641

while Fe_3O_4 MNPs stayed intact when the samples were heated up to 700 °C in an air flow.[60,61] Thus the Φ_{MNP} of PB20−C5MA$_{30}$−AA$_{116}$/MNP nanocomposite was determined from the weight percentage of the residue to be 3.2 wt %. The Φ_{MNP} values of PB20−C5MA$_{35}$−AA$_{76}$/MNP and PB20−C5MA$_{30}$−AA$_{223}$/MNP were also obtained from TGA (Figure S3 and S4, Supporting Information), and the results are listed in Table 2. For all the polymer/MNP nanocomposites, Φ_{MNP} is in the range of 3.2−5.3 wt % (Table 2).

Table 2. Weight Fraction of MNPs and MNP Micelles, LC to Isotropic Transition Temperature, and Corresponding Enthalpies of Polymer/MNP Nanocomposites

			T_i/°C (ΔH/J g^{-1})[c]	
nanocomposite	Φ_{MNP} (wt %)[a]	$\Phi_{micelles}$ (wt %)[b]	cooling	heating
PB20−C5MA$_{35}$−AA$_{76}$/MNP	4.6	9.8	139.5 (1.08)	146.5 (1.35)
PB20−C5MA$_{30}$−AA$_{116}$/MNP	3.2	4.6	135.7 (0.52)	143.1 (0.99)
PB20−C5MA$_{30}$−AA$_{223}$/MNP	5.3	nd	135.7 (0.46)	145.6 (0.73)

[a]Determined by TGA. [b]Calculated from Φ_{MNP} and the weight fraction of the polymer coating in the MNP micelles determined by TGA [c]Isotropization temperature and the corresponding enthalpy of the nanocomposite were determined by DSC at a ramping rate of 20 °C/min in the second heating and cooling cycle.

The $\Phi_{micelles}$ of polymer/MNP nanocomposite was calculated from Φ_{MNP} as the fraction of the polymer coating in the MNP micelles, namely, the amount of the polymers that were directly anchored to the MNPs was determined. For this purpose, MNP micelles were also collected and separated from the polymer/MNP solution using a magnet and dried in vacuo prior to TGA. Figure 4 shows the TGA traces of MNP micelles from PB20−C5MA$_{30}$−AA$_{116}$/MNP nanocomposite, in which the weight fraction of the MNPs encapsulated in the MNP micelles was found from the residue to be ∼70 wt %, implying that the fraction of the bonded polymer coating is ∼30 wt %. Combining this result with Φ_{MNP} = 3.2 wt %, $\Phi_{micelles}$ of PB20−C5MA$_{30}$−AA$_{116}$/MNP nanocomposite was calculated to be 4.6 wt %. Using the same procedure, $\Phi_{micelles}$ of PB20−C5MA$_{35}$−AA$_{76}$/MNP was also determined (Table 2). $\Phi_{micelles}$ of PB20−C5MA$_{30}$−AA$_{223}$/MNP could not be determined due to the lack of material.

Liquid Crystalline Ordering of the Polymer/MNP Nanocomposite. The presence of the LC ordering in the polymers/MNP nanocomposites is critical for the preparation of the swollen ferrogels, because upon swelling the PEO and PAA chains will be solvated in water, and the dehydrated LC domains can serve as junctions to uphold the integrity of the resulting ferrogel. Differential scanning calorimetry (DSC) was used to verify the presence of the LC phases in the pentablock copolymers PB20−C5MA$_x$−AA$_y$ and their corresponding polymer/MNP nanocomposites. In Figure 5, the DSC traces of pentablock copolymer PB20−C5MA$_{30}$−AA$_{116}$ and PB20−C5MA$_{30}$−AA$_{116}$/MNP nanocomposite are compared. It was observed that PB20−C5MA$_{30}$−AA$_{116}$/MNP displayed a lower LC to isotropic transition temperature (T_i) along with a more broadened transition peak compared to PB20−C5MA$_{30}$−AA$_{116}$, which can be attributed to the interaction between the included MNPs and the LC phase.[62,63] A similar broadening of the transition was also observed in the DSC traces for PB20−C5MA$_{35}$−AA$_{76}$/MNP and PB20−C5MA$_{30}$−AA$_{223}$/MNP (Figure S5, Supporting Information). Nevertheless, by keeping the content of the loaded MNPs relatively low (3.2−5.3 wt %), the LC phase was retained in all the prepared nanocomposites, and their T_i and corresponding transition enthalpies are summarized in Table 2.

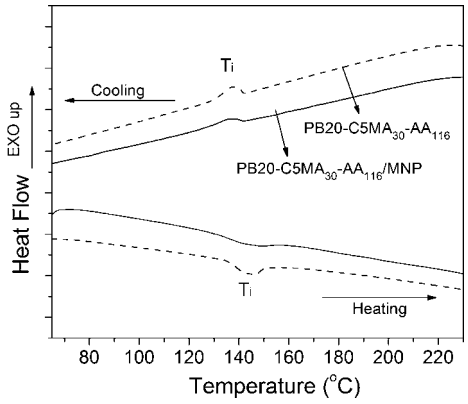

Figure 5. DSC traces of PB20−C5MA$_{30}$−AA$_{116}$ and PB20−C5MA$_{30}$−AA$_{116}$/MNP nanocomposite at a ramping rate of 20 °C/min in the second heating and cooling cycle.

The LC mesophase morphology in the pentablock copolymers and polymer/MNP nanocomposites was identified by 2D wide-angle X-ray scattering (2D WAXS). The obtained 2D WAXS patterns were converted to 1D diffractograms and are shown in Figure 6a. For the plain polymer PB20−C5MA$_{30}$−AA$_{116}$, a typical broad halo was observed at scattering vector q = 11.2 nm^{-1}, attributed to the lateral distance of the cholesteryl mesogens. Two diffraction peaks were observed at q = 2.4 and 3.7 nm^{-1} with a ratio of 2:3, and they are inferred to be the second- and third-order reflections of a smectic A phase. The primary LC reflection was calculated to be 1.2 nm^{-1} and matched reasonably well with the primary LC peak (q = 1.3 nm^{-1}) observed in small-angle X-ray scattering (SAXS) (Figure S7, Supporting Information). From Bragg's law, the d-spacing of the smectic A layers was calculated to be 5.2 nm, which is about twice the molecular length of the side-chain cholesteryl mesogens with the spacer (2.5 nm calculated with ChemBio 3D software). It can be concluded that PB20−C5MA$_{30}$−AA$_{116}$ has a bilayered smectic A structure (SmA_2), as illustrated in Figure 6b.[48] Two other peaks are observed at q = 13.1 and 16.1 nm^{-1}, which are the characteristic peaks for PEO crystallization.[48] Figure 6a also shows the diffractogram of PB20−C5MA$_{30}$−AA$_{116}$/MNP nanocomposite, in which similar LC ordering peaks was observed, indicating that the SmA_2 structure was retained regardless of the inclusion of the MNPs, which was correspondent to the DSC result. Furthermore, the appearance of the reflections at q = 21.0, 24.5, and 29.5 nm^{-1} (2θ = 30°, 35°, and 43°) confirmed the presence of Fe_3O_4 crystals.[53,61] WAXS studies have also been performed for PB20−C5MA$_{35}$−AA$_{76}$/MNP and PB20−C5MA$_{30}$−AA$_{116}$/MNP nanocomposites, in which SmA_2 mesophase has been identified.

Hierarchical Structure of the Polymer/MNP Nanocomposite. In the previous sections, the morphology of polymer/MNP nanocomposites composed of both the LC phase and the embedded MNP micelles has been investigated. The MNP clusters were encapsulated and stabilized by micelles formed by pentablock copolymers, and the MNP micelles possessed a multilayered structure where PAA-wrapped MNP clusters form the core, cholesteryl mesogens form the middle layer, and the

dx.doi.org/10.1021/ja208349x | J. Am. Chem.Soc. 2012, 134, 1630−1641

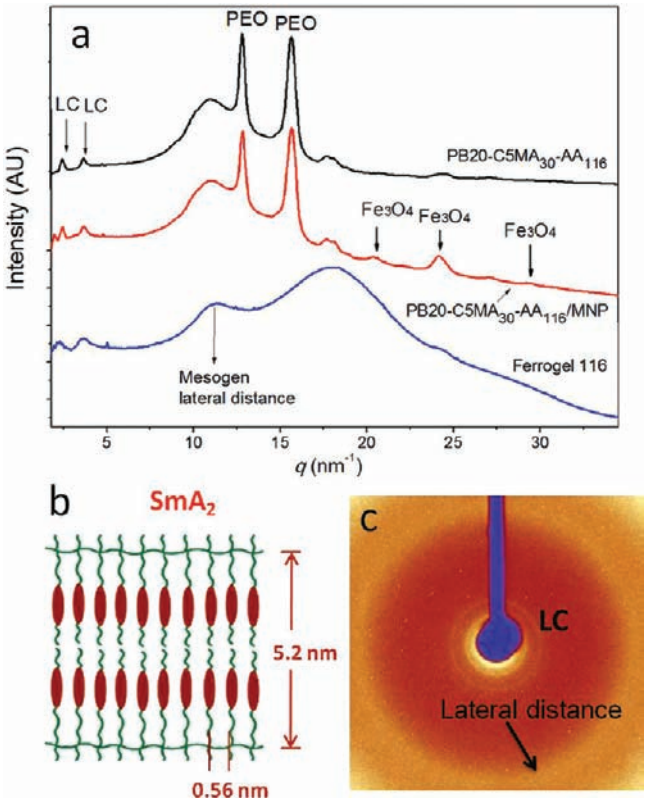

Figure 6. (a) 1D diffractograms of PB20−C5MA$_{30}$−AA$_{116}$, PB20−C5MA$_{30}$−AA$_{116}$/MNP nanocomposite, and ferrogel 116. (b) Schematic illustration of SmA$_2$ structure. (c) 2D WAXS pattern for ferrogel 116 (zoomed-in to show only the LC diffraction peaks and scattering of mesogen lateral distance).

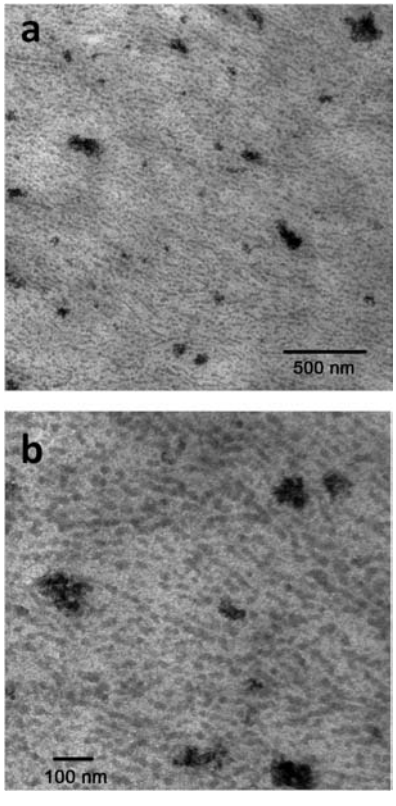

Figure 7. (a) Broad range TEM image and (b) zoomed-in TEM image of compression-molded PB20−C5MA$_{30}$−AA$_{116}$/MNP nanocomposite. The ultrathin cross-section sample was prepared by cryomicrotomy and stained with RuO$_4$ vapor.

PEO chains and the unreacted PAA segments formed the outer corona. Cholesteryl mesogens of the unbonded polymers self-assembled to form the SmA$_2$ phase which acts as a junction to connect the PEO and PAA blocks. Nevertheless, the complete picture as to how the MNP micelles and the LC domains are arranged in the polymer matrix remains to be identified. Therefore, the morphology of the compression-molded polymer/MNP nanocomposite has been studied by TEM. Ultrathin cross-section samples were prepared through a cryomicrotomy technique and stained with RuO$_4$ vapor. Figure 7a shows the TEM image of PB20−C5MA$_{30}$−AA$_{116}$/MNP nanocomposite. First, clusters of dark particles dispersed in polymer matrix determined to be MNPs were observed. Most MNP clusters are around 50−100 nm in diameter, which is correspondent to sizes of the MNP cluster found in the TEM of the polymer/MNP solution-cast sample. This implies that MNP micelles were essentially intact during the drying and compression molding because of the strong coordination bonding between the MNPs and PAA chains, with the exceptions of PAA and PEO chains, which collapsed/shrank due to the loss of water. Besides, a few large-size clusters (~200 nm in diameter) were also observed in Figure 7a, which could be attributed to the further agglomerating of the MNPs. Second, despite the presence of MNP clusters, it was observed that the polymer matrix also displays a block copolymer microsegregated structure. In the zoomed-in TEM image (Figure 7b), a mixture of circular-shaped and rod-like concentrations of electron density can be clearly discerned, which are identified to be the end-on and side-on view of cylinders. Since RuO$_4$ vapor preferentially stains PEO domains, and PEO and PAA chains likely merged together due to the hydrogen bonding, the cylindrical structures may be formed by PEO and PAA. The unstained background composed of PC5MA blocks has been identified to possess a SmA$_2$ phase by WAXS. It was also observed that at the positions where the MNP clusters are present, the microsegregated cylindrical structure was locally disturbed. Therefore, it can be seen that the melt sample of the PB20−C5MA$_{30}$−AA$_{116}$/MNP nanocomposite actually possessed a very complicated hierarchical structure, as depicted in Figure 8a. SAXS was also performed to further confirm the nanostructure of the polymer/MNP nanocomposite. However, due to the strong scattering caused by the MNPs, the diffraction peaks of the microsegregated structure were overridden and could not be located (Figure S7, Supporting Information). Detailed structure−property studies of the other two polymer/MNP nanocomposites will be conducted in the future.

Preparation and Study of the Gel Properties of the LC Ferrogels. By swelling the dry polymer/MNP nanocomposite samples in DI water, three-dimensional free-standing ferrogels were prepared. The discoid polymer/MNP nanocomposite samples prepared through compression molding were placed in DI water for at least 24 h to ensure that the swelling process had reached equilibrium (measured gravimetrically). The obtained water-swollen ferrogels were free-standing and do not need support from containers like conventional physical hydrogels, suggesting that the LC domains served as physical cross-linkers that were sufficiently strong to lead to mechanically robust hydrogels. The swollen ferrogel prepared

dx.doi.org/10.1021/ja208349x | J. Am. Chem.Soc. 2012, 134, 1630−1641

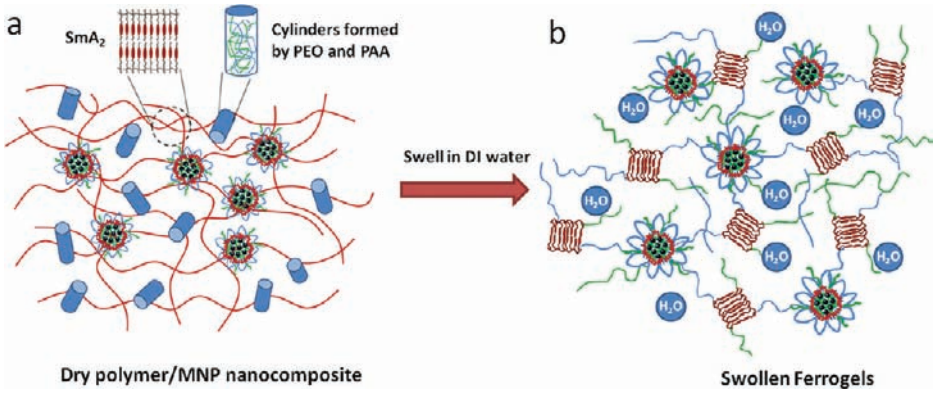

Figure 8. (a) Schematic illustration of the dry polymer/MNP nanocomposite with a hierarchical structure where MNP clusters were dispersed in microsegregated polymer matrix. (b) Schematic illustration of the swollen LC ferrogel with a network structure connected by LC domains and MNP clusters.

from PB20−C5MA$_x$−AA$_y$/MNP nanocomposite is labeled as "ferrogel *y*". Figure 9a shows the digital photos of the dry discoid samples of nanocomposites and the corresponding swollen ferrogels, which demonstrate the dimension change of the LC ferrogels compared to the original dry samples. A set of digital photos has also been included in the Supporting Information (Figure S6) that demonstrates that the prepared free-standing ferrogels were easily bent under compressive stress and recovered when the stress is released, suggesting good flexibility and elasticity.

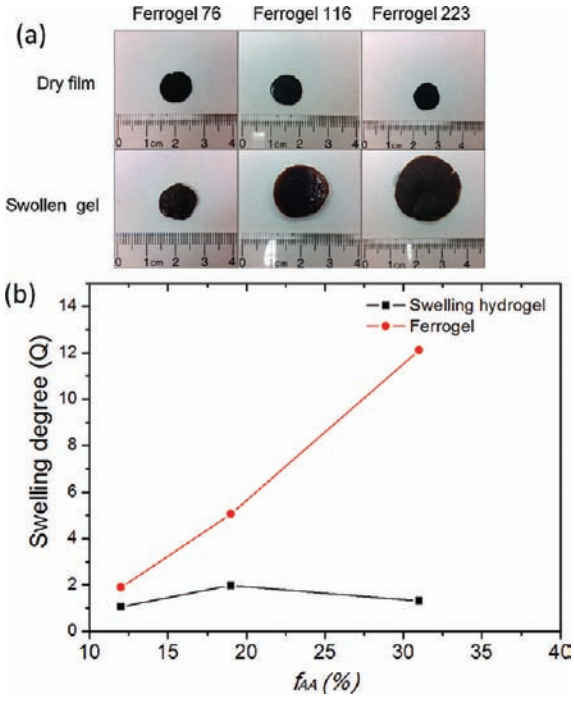

Figure 9. (a) Digital photos of the dry nanocomposite films and their corresponding ferrogels. (b) Swelling degree of LC ferrogels and plain polymer hydrogels versus weight fraction of AA.

Mesostructural Analysis of the Swollen Ferrogels. The swollen ferrogels were also studied by WAXS. The diffractogram of ferrogel 116 obtained by swelling PB20−C5MA$_{30}$−AA$_{116}$/MNP is shown in Figure 6a, in which the same LC diffraction peaks and scattering of mesogen lateral distance as the dry PB20−C5MA$_{30}$−AA$_{116}$/MNP nanocomposite were observed. This indicated that the hydrophobic LC domains preformed in the nanocomposite stayed dehydrated and intact during the swelling process. Furthermore, the disappearance of the PEO crystallization peaks was also observed for ferrogel 116, indicating complete solvation of PEO chains in water. In Figure 6c, the 2D WAXS pattern of ferrogel 116 also shows the LC diffraction rings and the scattering halo due to the mesogen lateral distance, though with relatively low intensities. The lack of intensity of the reflection peaks is due to the large water uptake and consequently low polymer content in the ferrogel sample. From the WAXS study it can be concluded that, upon the swelling of the polymer/MNP nanocomposites, the hydrophilic PEO and PAA chains absorbed water while the LC domains stayed intact and functioned as the physical cross-linkers or junctions to connect the solvated PEO and PAA chains.

It was difficult to perform TEM on the ferrogel sample due to retention of large amounts of water, and SAXS study was also not possible due the interference of the strong scattering from the included MNPs. Hence, direct structural analysis of the nanostructures of the ferrogels was not possible. Nevertheless, taking the PB20−C5MA$_{30}$−AA$_{116}$/MNP nanocomposite as the example, two possible scenarios regarding the structure of the swollen ferrogels can be reasonably inferred: (1) Upon swelling with water, the cylinders formed by hydrophilic PEO and PAA absorb water while the LC domains stayed intact (as shown by WAXS); the microsegregated cylindrical structure was essentially retained, although the PAA/PEO domain size increased due to the water uptake. (2) Due to the absorption of large amounts of water, the microsegregated PEO and PAA cylindrical domain size increased significantly and eventually the domain becomes a continuous phase; thus, the cylindrical morphology was completely disrupted, leading to a network structure connected by the LC domains as the physical cross-linkers. In the digital photos shown in Figure 9a, it can be seen that for PB20−C5MA$_{30}$−AA$_{116}$/MNP nanocomposite, the dimensions of the swollen ferrogel 116 was much bigger than that of the original dry sample (the diameter of the discoid sample increased about two times), due to the absorption of a large amount of water. It is unlikely that with this significant dimension increase the cylindrical PEO/PAA domains that have absorbed water can stay confined and separated in the LC matrix. Thus, the second hypothesis is more plausible, as illustrated in Figure 8b: the microsegregated structure in the melt state was disrupted by the absorption of

dx.doi.org/10.1021/ja208349x | *J. Am. Chem.Soc.* 2012, 134, 1630−1641

Table 3. Summary of the Composition and Swelling Properties of LC Ferrogels and Corresponding Plain Hydrogels

	f_{AA} (%)	LC ferrogel	$Q_{ferrogel}$[a]	$\mu_{polymer/ferrogel}$ (%)[b]	hydrogel	$Q_{hydrogel}$[a]	$\mu_{polymer/hydrogel}$ (%)[c]
PB20−C5MA$_{35}$−AA$_{76}$/MNP	12	ferrogel 76	1.9	33.4	hydrogel 76	1.0	48.8
PB20−C5MA$_{30}$−AA$_{116}$/MNP	19	ferrogel 116	5.1	15.7	hydrogel 116	2.0	33.6
PB20−C5MA$_{30}$−AA$_{223}$/MNP	31	ferrogel 223	12.1	7.2	hydrogel 223	1.3	43.1

[a]The swelling degree (Q) was calculated from eq 1. [b]The polymer concentration in the LC ferrogel was calculated from eq 2. [c]The polymer concentration in the plain hydrogel was calculated from eq 3.

water and the PEO/PAA domains morphed into continuous network connected by the LC domains. Upon swelling, the embedded MNPs will not be leached out, since they are anchored to the polymer network through coordination bonding. Furthermore, the MNP micelles may even serve as the second physical cross-linker in addition to the LC domains, since the cholesteryl mesogen layer in the MNP micelles may associate with the cholesteryl mesogens in the unbonded polymer chains due to the hydrophobic interaction.

Swelling Behaviors of the LC Ferrogels. The equilibrium swelling degree (Q) of the LC ferrogels was calculated according to eq 1,

$$Q = (W_s - W_d)/W_d \quad (1)$$

where W_s and W_d represent the weight of the swollen sample and the dry sample, respectively. The concentration of the polymer in the LC ferrogel ($\mu_{polymer/ferrogel}$) was calculated according to eq 2,

$$\mu_{polymer/ferrogel} = W_d/W_s \times (1 - \Phi_{MNP}) \quad (2)$$

Plain swollen hydrogels without MNPs were also prepared from native pentablock copolymers by using the same procedure for preparing ferrogels, and their swelling behaviors were compared with those of the corresponding LC ferrogels. The swollen hydrogel prepared from polymer PB20−C5MA$_x$−AA$_y$ is labeled as "hydrogel y". The swelling degree of plain hydrogels was calculated according to eq 1, while their polymer concentration ($\mu_{polymer/hydrogel}$) was calculated by using eq 3,

$$\mu_{polymer/hydrogel} = W_d/W_s \quad (3)$$

The swelling degrees and polymer concentrations of the prepared LC ferrogels and plain hydrogels are summarized in Table 3. The Q values for both the LC ferrogels and the plain hydrogels are plotted against the weight fraction of the PAA (f_{AA}) block in the pentablock copolymer (Figure 9b). From Figure 9b, it can be seen that, for the LC ferrogels, Q increased significantly with the increased f_{AA} in the polymer. Since all three pentablock copolymers used in this study have fixed PEO molecular weight (20K/mol) and narrow variation in LC block lengths (DP = 30−35) as well as the MNP content (3.2−5.3 wt %), this result demonstrated that the swelling degrees of the LC ferrogels were easily tuned by adjusting the PAA content in the pentablock copolymer. Interestingly we also observed that the Q values of the plain hydrogels were much lower than those of the corresponding ferrogels containing the same pentablock copolymers. It is known that the equilibrium swelling degree is the result of the balance between the osmotic driving force to dissolve as much hydrophilic polymer chains as possible (PEO and PAA in this case) and the entropy penalty of the polymer chain stretching to absorb more water.[46] Therefore, the different Q values of the plain hydrogels and LC ferrogels may be due to the different nanostructures possessed by the dry samples from which the hydrogels or ferrogels were prepared, which dictated the chain stretching of the PAA and PEO during the swelling process. As discussed in previous sections, the polymer/MNP nanocomposite possessed a microsegregated structure (i.e., cylindrical morphology for PB20−C5MA$_{30}$−AA$_{116}$/MNP nanocomposite) with embedded MNP micelles; at the positions where the MNP micelles are located, the microsegregation was locally disrupted. In contrast, for the plain polymer samples without MNPs, the block copolymer microphase separation may be more well-defined and therefore the chain stretching of the PAA and PEO blocks may be more constrained by the LC domains, resulting in lower swelling degrees. The hypothesis will be tested in the future using different morphological tools.

Mechanical Properties of LC Ferrogels and Plain Hydrogels. Good mechanical properties are required for hydrogels used in soft actuator applications.[64] Especially for biological applications such as artificial muscles or tissue engineering scaffolds, hydrogels with mechanical properties compatible with natural tissues having moduli (G') around 10^4−10^5 Pa are often desired.[65] To evaluate the mechanical strength of the swollen LC ferrogels, oscillatory frequency sweep experiments have been conducted at 25 °C under constant stress. The mechanical properties of plain hydrogels have also been studied as the control to investigate the influence of the included MNPs on the mechanical properties of the LC ferrogels.

Figure 10a shows the storage modulus G' and the loss modulus G'' of both ferrogel 116 and hydrogel 116 as a function of angular frequency. For ferrogel 116, G' was larger than G'' across the entire frequency range and G' was independent of the frequency, indicating the high degree of elasticity of the ferrogel. It was noticed that, although the polymer concentration in the ferrogel 116 (15.7 wt %) was much lower than that in hydrogel 116 (33.6 wt %), the G' of the former was similar to that of the latter. This may be due to MNPs directly bonded to the polymer network functioning as metallic fillers and possibly as secondary physical cross-linkers in addition to the LC domains, and these synergistic roles of both MNP and LCs enhanced the mechanical properties of the ferrogel. A similar effect of the MNPs was also observed in ferrogel 76 with 33.4 wt % of polymer and hydrogel 76 with 48.8 wt % of polymer (Figure S8, Supporting Information). In contrast, Figure 10b shows that the G' of ferrogel 223 was lower than the G' of hydrogel 223 by about half an order of magnitude. This is because of the drastically increased swelling degree of the ferrogel 223 after the inclusion of MNPs and much lower polymer concentration (7.2 wt %) compared to that of hydrogel 223 (43.1 wt %). Although the included MNPs served as the physical cross-linkers/fillers in ferrogel 223, their influence was not sufficient to compensate for the reduced mechanical strength caused by the lower amount of polymer.

The dynamic frequency sweep experiment results of the LC ferrogels are compared in Figure 10c, in which the plateau behavior of G' was observed for all the samples, indicating their high elasticity. Also, G' of the ferrogels decreased with the

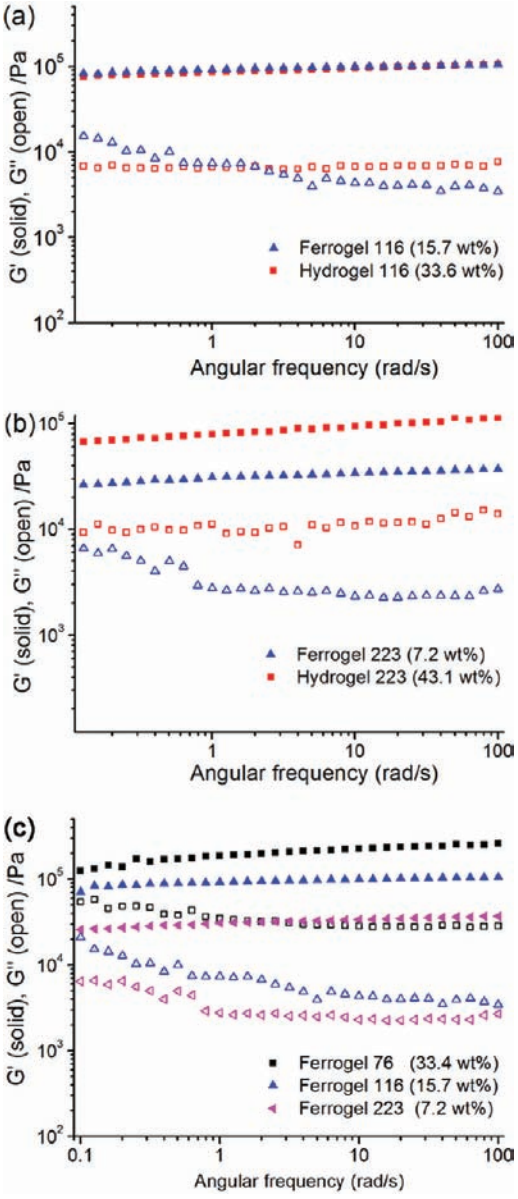

Figure 10. Dynamic frequency sweep of (a) ferrogel 116 and hydrogel 116 and (b) ferrogel 223 and hydrogel 223. (c) Comparison of dynamic frequency sweep experiments of all the LC ferrogels.

increased PAA block length in the pentablock copolymers. This is attributed to the fact that increasing the PAA block length leads to larger water uptake and subsequently lower polymer concentration in the resulting ferrogels. Furthermore, increasing the PAA block length also altered the compositions of the pentablock copolymers. This may also lead to different nanostructures of the polymer/MNP nanocomposites, which may influence the mechanical strength of the resulting ferrogels.

Nevertheless, it is important to note that for ferrogel 223 with only 7.2 wt % of polymer, the G' is around 3×10^4 Pa, and for ferrogel 116 with 15.7 wt % of polymer, the G' value is around 7×10^4 Pa. Typical physical hydrogels with similar or higher polymer concentrations usually display much lower G' values compared to the ferrogels prepared here. For instance, for a physical hydrogel formed by Pluronic F127 at room temperature with polymer concentration of 20 wt %, the G' value ($7\sim8$) $\times 10^3$ Pa) is about an order of magnitude lower than that of ferrogel 116 ($\sim 7 \times 10^4$ Pa).[66] In another example, Tew et al. have prepared a physical hydrogel of PLA–PEO–PLA with 16 wt % of polymer, which also exhibits a lower G' value ($\sim 1 \times 10^4$ Pa) compared to ferrogel 116 or ferrogel 223.[65] Thus, in the current study, ferrogels with mechanical strength comparable with chemically cross-linked hydrogels but higher than previously reported physical ferrogel systems (hydrogel or organogel based) have been obtained.[41−44] The enhanced mechanical properties of the LC ferrogels should be attributed to the synergistic effect of both the LC domains, which serve as effective physical cross-linkers, and the embedded MNP micelles, which serve as metallic fillers and possibly the second physical cross-linkers. These swollen LC ferrogels with storage moduli comparable with those of natural soft tissues ($G' = 10^4$–10^5 Pa) are promising candidates for applications including artificial muscles and tissue engineering scaffolds.

Actuation of LC Ferrogel Using Magnetic Field. To evaluate the ability of these LC ferrogel to function as soft magnetic actuators, actuation experiments were conducted. As shown in Figure 11, a rectangular stripe sample (2.5 cm × 0.2 cm) was cut from the ferrogel 116 film. One end of the LC ferrogel stripe was immobilized by sandwiching a small portion of it between two glass slides, so that the major portion of the stripe was free to be bent. A magnet was used to provide a moderate inhomogeneous magnetic field. When the magnet was moved close to the ferrogel stripe, the stripe bent because of the magnetic attraction, and when the magnet was moved away, the stripe recovered to its original shape and position. A video clip of this actuation experiment is included in the Supporting Information, in which one can clearly observe that the response of the LC ferrogel appears to be fast and reversible. The process was repeated many times, indicating the mechanical stability and flexibility of the LC ferrogel.

■ CONCLUSION

In this study we have demonstrated a unique strategy leading to hierarchically structured physically cross-linked ferrogels through the swelling of a series of polymer/MNP nanocomposites composed of amphiphilic LC pentablock copolymer PB20−C5MA$_x$−AA$_y$ and Fe_3O_4-based MNPs. The melt sample of the polymer/MNP nanocomposite possessed a hierarchical structure, in which micelles encapsulating MNP clusters are embedded in the polymer matrix, and the polymer matrix adopts a cylindrical morphology with cylinders formed

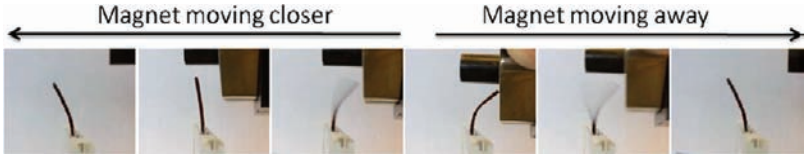

Figure 11. Actuation of LC ferrogel 116 using a magnet.

dx.doi.org/10.1021/ja208349x | J. Am. Chem.Soc. 2012, 134, 1630−1641

by PEO/PAA chains dispersed in the LC matrix. Upon swelling with water, the hydrophilic PEO and PAA chains absorbed large amounts of water and transformed into a continuous network, while the LC domains stayed dehydrated and functioned as the physical cross-linkers to connect the hydrogel network, leading to free-standing LC ferrogels. The embedded MNP clusters were anchored to the polymer network via coordination bonding so that they will not be leached out during swelling. Moreover, the MNP micelles may even function as the second physical cross-linkers, since cholesteryl mesogen layer surrounding the MNPs may associate with the cholesteryl mesogens from the polymer matrix. The resulting free-standing ferrogels displayed good mechanical properties, with storage moduli G' ranging between 10^4 and 10^5 Pa, attributed to the LC domains and the embedded MNPs. By altering the PAA block length in the pentablock copolymer, both the swelling degree in water and G' of the ferrogels were tuned. Furthermore, application of a magnetic field induced fast and reversible bending actuation of the prepared ferrogel sample. Therefore, these physically cross-linked free-standing LC ferrogel featuring good mechanical properties, tunable swelling degrees, and superparamagnetic properties are good candidates for soft actuators and artificial muscles. In the future, these hierarchically structured ferrogel networks can be exploited for encapsulation and delivery of hydrophobic drugs by deformation or remotely heating of MNPs using alternating magnetic fields. This multifunctional pentablock copolymer scaffold provides a versatile modular approach to template various nanoparticles (metallic, inorganic, biological, etc.) and produce robust free-standing hybrid hydrogels with unique magnetic, electric, optical, multiresponsive, or bioactive properties.

■ ASSOCIATED CONTENT

Supporting Information

Experimental procedures; additional figures including ^{1}H NMR spectra, GPC traces, and SAXS diffractograms; and a video clip of the actuation experiment. This material is available free of charge via the Internet at http://pubs.acs.org.

■ AUTHOR INFORMATION

Corresponding Author

Kasi@ims.uconn.edu

■ ACKNOWLEDGMENTS

Financial support was provided by the University of Connecticut New-Faculty Start-up Fund, University of Connecticut Research Foundation Faculty Grant, NSF CAREER Award to R.M.K. (DMR-0748398) and NSF grant (#1105975) to M.J. Central instrumentation facilities of the Institute of Materials Science and Chemistry Department and the TEM facility at Physiology and Neurobiology (PNB) are also are acknowledged. We also thank Stephen Daniels for sectioning samples and performing TEM experiments and Marie Cantino for useful discussions. We are very thankful to the NSF-MRSEC X-ray Scattering Laboratory at University of Massachusetts Amherst for using their Rigaku-Molmet SAXS–WAXS equipment for our SAXS data collection, to Dr. Dhanasekaran Thirunavukkarasu for helpful assistance, and for a NSF-MRSEC Materials Research Facilities Network Grant to cover the user fee.

■ REFERENCES

(1) Kopeček, J.; Yang, J. *Polym. Int.* **2007**, *56*, 1078–1098.
(2) Ahn, S.-K.; Kasi, R. M.; Kim, S. C.; Sharma, N.; Zhou, Y. *Soft Matter* **2008**, *4*, 1151–1157.
(3) Yamaguchi, N.; Zhang, L.; Chae, B. S.; Palla, C. S.; Furst, E. M.; Kiick, K. L. *J. Am. Chem. Soc.* **2007**, *129*, 3040–3041.
(4) Yang, H.; Liu, H.; Kang, H.; Tan, W. *J. Am. Chem. Soc.* **2008**, *130*, 6320–6321.
(5) Hu, Z.; Chen, Y.; Wang, C.; Zheng, Y.; Li, Y. *Nature* **1998**, *393*, 149–152.
(6) Kwon, I. C.; Bae, Y. H.; Kim, S. W. *Nature* **1991**, *354*, 291–293.
(7) Mortensen, K.; Brown, W.; Joergensen, E. *Macromolecules* **1994**, *27*, 5654–5666.
(8) Li, Y.; Narain, R.; Ma, Y.; Lewis, A. L.; Armes, S. P. *Chem. Commun.* **2004**, 2746–2747.
(9) Yuk, S. H.; Cho, S. H.; Lee, S. H. *Macromolecules* **1997**, *30*, 6856–6859.
(10) Iddon, P. D.; Armes, S. P. *Eur. Polym. J.* **2007**, *43*, 1234–1244.
(11) Hamilton, T. D.; Buc ar, D. K.; Baltrusaitis, J.; Flanagan, D. R.; Li, Y.; Ghorai, S.; Tivanski, A. V.; MacGillivray, L. R. *J. Am. Chem. Soc.* **2011**, 3365–3371.
(12) Bayazit, M. K.; Clarke, L. S.; Coleman, K. S.; Clarke, N. *J. Am. Chem. Soc.* **2010**, 15814–15819.
(13) Takafuji, M.; Yamada, S.; Ihara, H. *Chem. Commun.* **2011**, 1024–1026.
(14) Tokarev, I.; Tokareva, I.; Minko, S. *Adv. Mater.* **2008**, *20*, 2730–2734.
(15) Ince, G. O.; Demirel, G.; Gleason, K. K.; Demirel, M. C. *Soft Matter* **2010**, *6*, 1635–1639.
(16) Gawel, K.; Stokke, B. T. *Soft Matter* **2011**, 4615–4618.
(17) Thilakarathne, V.; Briand, V. A.; Zhou, Y.; Kasi, R. M.; Kumar, C. V. *Langmuir* **2011**, *27*, 7663–7671.
(18) Hu, S.-H.; Liu, T.-Y.; Liu, D.-M.; Chen, S.-Y. *Macromolecules* **2007**, *40*, 6786–6788.
(19) Wu, J.; Gong, X.; Fan, Y.; Xia, H. *Soft Matter* **2011**, *7*, 6205–6212.
(20) Ramanujan, R.; Lao, L. *Smart Mater. Struct.* **2006**, *15*, 952–956.
(21) Krekhova, M.; Lang, T.; Richter, R.; Schmalz, H. *Langmuir* **2010**, *26*, 19181–19190.
(22) Zhao, X.; Kim, J.; Cezar, C. A.; Huebsch, N.; Lee, K.; Bouhadir, K.; Mooney, D. J. *Proc. Natl. Acad. Sci. U. S. A.* **2011**, *108*, 67–72.
(23) Mayer, C. R.; Cabuil, V.; Lalot, T.; Thouvenot, R. *Adv. Mater.* **2000**, *12*, 417–420.
(24) Szabo, D.; Szeghy, G.; Zrinyi, M. *Macromolecules* **1998**, *31*, 6541–6548.
(25) Xulu, P. M.; Filipcsei, G.; Zrinyi, M. *Macromolecules* **2000**, *33*, 1716–1719.
(26) Galicia, J.; Cousin, F.; Dubois, E.; Sandre, O.; Cabuil, V.; Perzynski, R. *Soft Matter* **2009**, *5*, 2614–2624.
(27) Fuhrer, R.; Athanassiou, E. K.; Luechinger, N. A.; Stark, W. J. *Small* **2009**, *5*, 383–388.
(28) Messing, R.; Frickel, N.; Belkoura, L.; Strey, R.; Rahn, H.; Odenbach, S.; Schmidt, A. M. *Macromolecules* **2011**, 2990–2999.
(29) Frickel, N.; Messing, R.; Gelbrich, T.; Schmidt, A. M. *Langmuir* **2010**, *26*, 2839–2846.
(30) Bonini, M.; Lenz, S.; Giorgi, R.; Baglioni, P. *Langmuir* **2007**, *23*, 8681–8685.
(31) Barbucci, R.; Pasqui, D.; Giani, G.; De Cagna, M.; Fini, M.; Giardino, R.; Atrei, A. *Soft Matter* **2011**, 5558–5565.
(32) Mathur, A. M.; Moorjani, S. K.; Scranton, A. B. *J. Macromol. Sci. Part A: Polym. Rev.* **1996**, *36*, 405–430.
(33) Jeong, B.; Bae, Y. H.; Lee, D. S.; Kim, S. W. *Nature* **1997**, *388*, 860–862.
(34) Shim, M. S.; Lee, H. T.; Shim, W. S. S.; Park, I.; Lee, H.; Chang, T.; Kim, S. W.; Lee, D. S. *J. Biomed. Mater. Res.* **2002**, *61*, 188–196.
(35) Shah, N. M.; Michael, D.; Metters, A. T. *Biomacromolecules* **2006**, *7*, 3171–3177.
(36) Kang, J.; Beers, K. J. *Biomacromolecules* **2006**, *7*, 453–458.

(37) Appel, E. A.; Biedermann, F.; Rauwald, U.; Jones, S. T.; Zayed, J. M.; Scherman, O. A. *J. Am. Chem. Soc.* **2010**, *132*, 14251−14260.
(38) van de Manakker, F.; Vermonden, T.; el Morabit, N.; van Nostrum, C. F.; Hennink, W. E. *Langmuir* **2008**, *24*, 12559−12567.
(39) Choi, H. S.; Huh, K. M.; Ooya, T.; Yui, N. *J. Am. Chem. Soc.* **2003**, *125*, 6350−6351.
(40) Tomatsu, I.; Hashidzume, A.; Harada, A. *J. Am. Chem. Soc.* **2006**, *128*, 2226−2227.
(41) Lattermann, G.; Krekhova, M. *Macromol. Rapid Commun.* **2006**, *27*, 1373−1379.
(42) An, H.; Picken, S. J.; Mendes, E. *Soft Matter* **2010**, *6*, 4497−4503.
(43) Roubeau, O.; Colin, A.; Schmitt, V.; Clérac, R. *Angew. Chem., Int. Ed.* **2004**, *43*, 3283−3286.
(44) Qin, J.; Asempah, I.; Laurent, S.; Fornara, A.; Muller, R. N.; Muhammed, M. *Adv. Mater.* **2009**, *21*, 1354−1357.
(45) Lee, K. Y.; Mooney, D. J. *Chem. Rev.* **2001**, *101*, 1869−1880.
(46) Guo, C.; Bailey, T. S. *Soft Matter* **2010**, *6*, 4807−4818.
(47) He, Y.; Lodge, T. *Chem. Commun.* **2007**, *2007*, 2732−2734.
(48) Zhou, Y.; Ahn, S.-K.; Lakhman, R. K.; Gopinadhan, M.; Osuji, C. O.; Kasi, R. M. *Macromolecules* **2011**, *44*, 3924−3934.
(49) Hsing, C. Y.; Pei, W. W.; Xu, R. Q.; Pei, J. *Fundamental Organic Chemistry*; 3rd ed.; Higher Education Press: Beijing, China, 2005.
(50) Lee, D.-Y.; Seo, J.-M.; Khan, W.; Kornfield, J. A.; Kurji, Z.; Park, S.-Y. *Soft Matter* **2010**, *6*, 1964−1970.
(51) Li, Y.; Zhang, Y.; Yang, D.; Hu, J.; Feng, C.; Zhai, S.; Lu, G.; Huang, X. *Macromolecules* **2009**, *43*, 262−270.
(52) Colombani, O.; Ruppel, M.; Schubert, F.; Zettl, H.; Pergushov, D. V.; Müller, A. H. E. *Macromolecules* **2007**, *40*, 4338−4350.
(53) Harris, L.; Goff, J.; Carmichael, A.; Riffle, J.; Harburn, J.; Pierre, T. G. S.; Saunders, M. *Chem. Mater.* **2003**, *15*, 1367−1377.
(54) Ditsch, A.; Laibinis, P. E.; Wang, D. I. C.; Hatton, T. A. *Langmuir* **2005**, *21*, 6006−6018.
(55) Kim, G. C.; Li, Y. Y.; Chu, Y. F.; Cheng, S. X.; Zhuo, R. X.; Zhang, X. Z. *Eur. Polym. J.* **2008**, *44*, 2761−2767.
(56) Zhang, Q.; Thompson, M. S.; Carmichael-Baranauskas, A. Y.; Caba, B. L.; Zalich, M. A.; Lin, Y. N.; Mefford, O. T.; Davis, R. M.; Riffle, J. S. *Langmuir* **2007**, *23*, 6927−6936.
(57) Lee, J.; Isobe, T.; Senna, M. *Colloids Surf. A* **1996**, *109*, 121−127.
(58) Gass, J.; Poddar, P.; Almand, J.; Srinath, S.; Srikanth, H. *Adv. Funct. Mater.* **2006**, *16*, 71−75.
(59) Zhang, Y. J.; Lin, Y. W.; Chang, C. C.; Wu, T. M. *Synth. Met.* **2010**, *160*, 1086−1091.
(60) Wuang, S. C.; Neoh, K. G.; Kang, E. T.; Pack, D. W.; Leckband, D. E. *J. Mater. Chem.* **2007**, *17*, 3354−3362.
(61) Qiu, G.; Wang, Q.; Nie, M. *Macromol. Mater. Eng.* **2006**, *291*, 68−74.
(62) Song, H. M.; Kim, J. C.; Hong, J. H.; Lee, Y. B.; Choi, J.; Lee, J. I.; Kim, W.; Kim, J. H.; Hur, N. *Adv. Funct. Mater.* **2007**, *17*, 2070−2076.
(63) Zadoina, L.; Lonetti, B.; Soulantica, K.; Mingotaud, A. F.; Respaud, M.; Chaudret, B.; Mauzac, M. *J. Mater. Chem.* **2009**, *19*, 8075−8078.
(64) Calvert, P. *Adv. Mater.* **2009**, *21*, 743−756.
(65) Aamer, K. A.; Sardinha, H.; Bhatia, S. R.; Tew, G. N. *Biomaterials* **2004**, *25*, 1087−1093.
(66) Fusco, S.; Borzacchiello, A.; Netti, P. A. *J. Bioact. Compat. Polym.* **2006**, *21*, 149−164.